

# Kinetic Monte Carlo simulations of 1D and 2D traffic flows: Comparison of two look-ahead potentials

Yi Sun\*

*Department of Mathematics and Interdisciplinary Mathematics Institute,  
University of South Carolina, Columbia, SC 29208, USA*

Ilya Timofeyev†

*Department of Mathematics, University of Houston, Houston, TX 77204, USA*

(Dated: June 5, 2013)

We employ an efficient list-based kinetic Monte Carlo (KMC) method to study a traffic flow model on one-dimensional (1D) and two-dimensional (2D) lattice based on Arrhenius microscopic dynamics. This model implements stochastic rules for the movement of cars based on the energy profile of the traffic ahead of each car. In particular, we compare two different look-ahead rules: one is based on the distance from the car under consideration to the car in front of it, the other one is based on the density of cars ahead. The 1D numerical results of these two rules show different coarse-grained macroscopic limits in the form of integro-differential Burgers equations. The 2D results of both rules exhibit a sharp phase transition from freely flowing to fully jammed, as a function of initial density of cars. The KMC simulations reported in this paper are compared with those from other well-known traffic flow models and the corresponding empirical results from real traffic.

PACS numbers: 89.40.-a, 05.50.+q, 64.60.-i, 02.70.-c

## I. INTRODUCTION

In the past few decades, traffic problems have attracted considerable attention of many scientists. It has been a fundamental task to model traffic flows for understanding the mechanisms leading to traffic jams and designing traffic networks for efficient transportation systems. A number of theoretical and computational models have been proposed to study traffic flows by using the methods and concepts of non-equilibrium statistical physics. These models can be roughly divided into several categories (see review papers or books [1–6] and references therein): (i) microscopic *discrete lattice* models (or individual-agent-based models) where a lattice site configuration with values 1 (car is present) and 0 (car is absent) combined with explicit rules for car movement on lattice sites is used to represent traffic flow; (ii) microscopic non-integer *car-following* models that treat cars as particles and use ordinary differential equations (possibly with delay) to describe the motion of cars; (iii) mesoscopic models that use kinetic theories to describe the probabilistic distribution of the car velocity, the moments of which give the macroscopic car density and flux; (iv) macroscopic models that treat the traffic flow as a compressible fluid formed by the cars and use partial differential equations (PDE, typically conservation laws) to relate the car density and flux.

In the microscopic models above, attention is explicitly focused on individual cars and the interactions among them are determined by the way the cars influence each

others' movements. While car-following models, such as the *follow-the-lead* model [7] and the *optimal velocity* model [8, 9], provide a more realistic setup allowing for detailed interaction rules, mechanisms for lane changing, etc., lattice models are simpler to implement and are more amenable to analytical investigation. Therefore, lattice models, such as the *cellular automaton* (CA) [10–18], have been widely used to represent traffic flow and a vast literature exists addressing various analytical and numerical techniques for models of this type. Recently, a novel look-ahead potential was introduced to model long-range interactions in prototype lattice model, which were then coarse-grained to obtain macroscopic descriptions [19, 20]. In particular, in [21] the look-ahead potential was used to model the effect of long-range traffic conditions and a new macroscopic PDE model with non-local interactions was formally derived. Extensions to multi-lane traffic have also been developed [22, 23]. An improved coarse-grained model at the ODE level has been made in [24].

In this paper we study a traffic flow model on one-dimensional (1D) and two-dimensional (2D) lattice which describes the interactions between cars by a look-ahead rule based on the energy profile of the traffic ahead of each car. In particular, we consider two different look-ahead rules: one is based on the distance from the car under consideration to the car in front of it, the other one is based on the density of cars ahead as used in [21]. Numerically we employ the kinetic Monte Carlo (KMC) algorithm [25] to simulate the microscopic stochastic dynamics of the traffic flow based on the Arrhenius law with these rules. One reason to choose KMC instead of the Metropolis Monte Carlo method [26] is that the KMC method can provide the transition rates which are asso-

---

\* yisun@math.sc.edu

† ilya@math.uh.edu

ciated with possible configurational changes of the traffic system, and then the corresponding time evolution of the system can be expressed in terms of these rates. Moreover, when the dynamics of the traffic system features a finite number of distinct processes in configurational changes, we develop an efficient list-based KMC algorithm using fast search that can further improve computational efficiency compared to the general KMC method.

The model parameters in the KMC method are calibrated against empirical results from real traffic. After calibration, the KMC simulations are used to quantitatively predict the time evolution of 1D and 2D traffic flows. The 1D numerical results of these two rules show different coarse-grained macroscopic limits in the form of integro-differential Burgers equations. The 2D results of both rules exhibit a sharp phase transition from freely flowing to fully jammed, as a function of initial density of cars. The results of our model are comparable to those from other well-known traffic flow models and the corresponding empirical results from real traffic in certain parameter regimes.

The rest of the paper is organized as follows. In Section 2, we introduce the lattice model with two look-ahead rules. In Section 3, we describe the list-based KMC algorithm and its implementation. In Section 4, we provide a series of numerical simulations in various parameter regimes on 1D and 2D lattice, respectively. We state our conclusion in Section 5.

## II. A LATTICE MODEL WITH LOOK-AHEAD RULES

We discuss the construction of the discrete lattice model for 1D traffic flow in this section. For simplicity, we assume that cars are forced to move toward one direction on a 1D periodic (single-lane loop highway with no entrances or exits) lattice  $\mathcal{L}$  partitioned into  $M$  evenly spaced cells,  $\mathcal{L} = \{1, 2, \dots, M\}$ . The configuration at each site  $x \in \mathcal{L}$  is defined by an index  $\sigma_x$ :

$$\sigma_x = \begin{cases} 1 & \text{if a car occupies cell } x, \\ 0 & \text{if the cell is empty,} \end{cases} \quad (1)$$

and the state of the system is represented by the configuration space  $\{0, 1\}^M$  with the element denoted by  $\sigma_x$ . In the following we label the cars in driving direction to the right such that the  $(n+1)$ -th vehicle is in front of the  $n$ -th car. Transitions in the state of system represent the car movements, which obey the rules of an exclusion process [27]: two nearest neighbor lattice sites exchange values in each transition and cars cannot occupy the same cell. In addition cars are only allowed to move one cell to the right in one transition. Therefore, the only possible configuration changes are of the form (see Fig. 1)

$$\{\sigma_x = 1, \sigma_{x+1} = 0\} \rightarrow \{\sigma_x = 0, \sigma_{x+1} = 1\}$$

The transition rate depends on spatial forward Arrhenius-type interactions with one-sided potentials

and a look-ahead feature which can be considered to represent driver behavior. This rule allows cars (or drivers) to perceive the traffic situation up to  $L$  cells ahead in which  $L$  is the look-ahead parameter. The interactions between a pair of successive cars cannot be neglected if the gap between them is shorter than  $L$ ; in such situations the following car must decelerate so as to avoid collision with the leading car. Similar to the spin-exchange Arrhenius dynamics in which the simulation is driven based on the energy barrier a particle has to overcome in changing from one state to another [21], we perform a car move only if the potential energy of the car is higher than a given threshold. The move is taken as a nearest-neighbor hopping process with its rate given by the Arrhenius relation:

$$r = \omega_0 \exp(-E_b) \quad (2)$$

where the prefactor  $\omega_0 = 1/\tau_0$  corresponds to the car moving frequency with  $\tau_0$  the characteristic or relaxation time. The moving energy barrier  $E_b$  is assumed to depend only on the local environment of the car under consideration up to range  $L$  ahead of it, which enforces the look-ahead rule (Fig. 1). In the following, we describe two different look-ahead rules.

The first one is based on the distance from the car under consideration to the car in front of it, in other words, the number of vacancy cells,  $N_v$ , between these two cars (as shown in left panels in Fig. 1). In particular, the energy barrier is given by

$$E_b = E_s + \frac{(L - N_v)}{L} E_c \quad (3)$$

where  $E_s$  is the energy associated with the site binding of the car, which could vary in both space and time to account for spatial and temporal traffic situations (in this study we set to  $E_s = 0$ ). The parameter  $E_c$  is the car look-ahead interaction potential strength. Then all cars can be classified into  $(L+1)$  folds according to their corresponding values of  $N_v$  ( $N_v = 0, 1, \dots, L$ ). Based on the formulas (2) and (3), we can see that the larger is the value of  $N_v$ , the smaller is the energy barrier  $E_b$ , thus the larger is the transition rate  $r$ . This reflects the fact that the closer is the distance between cars, the stronger is the slowdown factor.

From experience with real traffic we know that drivers usually observe not only the leading car but also other cars ahead of the leading car. Therefore, we also consider another look-ahead rule which is based on the density of cars ahead of the car under consideration [21]. In this rule, the energy barrier is given by

$$E_b = E_s + \frac{N_c}{L} E_c \quad (4)$$

where  $E_s$  and  $E_c$  are defined as above (in this study we set to  $E_s = 0$ ). As shown in the right panels in Fig. 1,  $N_c$  is the number of cars in the range  $L$  ahead of the car under consideration. Then all cars can also be classified

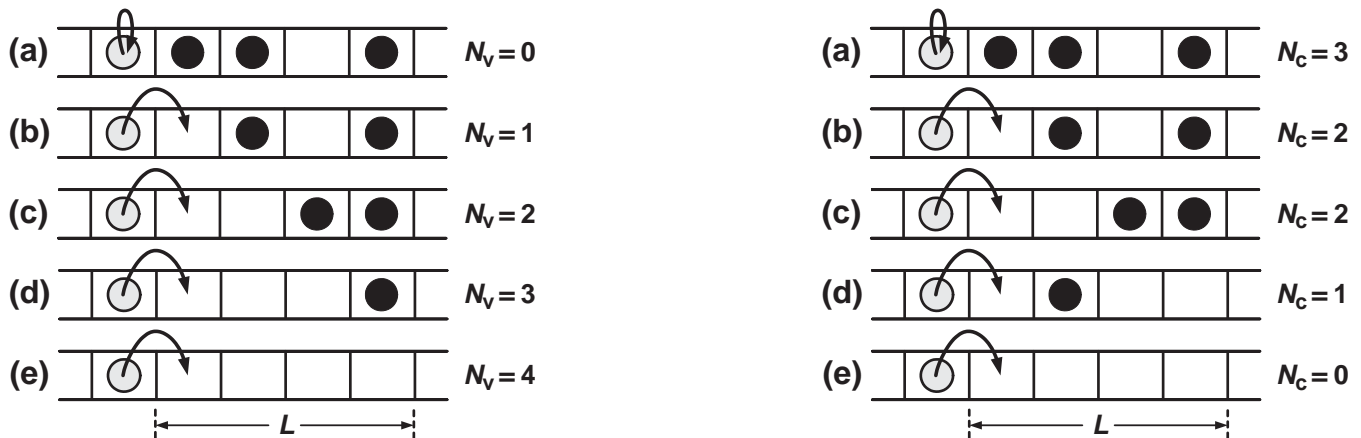


FIG. 1. Schematic representation of two look-ahead rules. (Left panels): The rule based on the distance: a car in gray with different numbers ( $N_v$ ) of vacancy cells between it and the first car ahead of it in the range  $L$  (here,  $L = 4$ ), (a):  $N_v = 0$ ; (b):  $N_v = 1$ ; (c):  $N_v = 2$ ; (d):  $N_v = 3$ ; (e):  $N_v = 4$ . (Right panels): The rule based on the density: a car in gray with different numbers ( $N_c$ ) of cars ahead of it in the range  $L$ , (a):  $N_c = 3$ ; (b):  $N_c = 2$ ; (c):  $N_c = 2$ ; (d):  $N_c = 1$ ; (e):  $N_c = 0$ .

into  $(L + 1)$  folds according to their corresponding values of  $N_c$  ( $N_c = 0, 1, \dots, L$ ). This look-ahead rule with the formula (4) indicates that a slowdown factor is stronger when the forward car density is high, i.e., when the road is congested.

To summarize, the following parameters need to be given for the stochastic simulations with either look-ahead rule: (i) the characteristic or relaxation time  $\tau_0$ ; (ii) the car interaction potential strength  $E_c$ ; and (iii) the look-ahead parameter  $L$ .

### III. THE KINETIC MONTE CARLO METHOD

We apply the kinetic Monte Carlo (KMC) method to the above lattice model to investigate the evolution of a traffic system. We choose KMC instead of the Metropolis Monte Carlo (MMC) method [26] since in the MMC method, trial steps are sometimes rejected because the acceptance probability is small, in particular when a system approaches the equilibrium, or the density of cars is high. The KMC method that we adopt here is related to the method proposed by Bortz, Kalos, and Lebowitz as a speed-up to the MMC method for simulating the evolution of Ising models [25]. A main feature of the KMC algorithm is that it is “rejection-free”. In each step, the transition rates for all possible changes from the current configuration are calculated and then a new configuration is chosen with a probability proportional to the rate of the corresponding transition. Since the interaction is short-ranged within the look-ahead distance, there is only a small number of local environments that need to be changed due to the previous transition. The other feature of KMC is its capability of simulating the dynamics of the system in real time. Since the corresponding time evolution is expressed in terms of these

rates, KMC should provide a more accurate description of time evolution of a traffic system than MMC.

The KMC algorithm is built on the assumption that the model features  $N$  independent Poisson processes (corresponding to  $N$  moving cars on the lattice) with transition rates  $r_i$  in (2) that sum to give the total rate  $R = \sum_{i=1}^N r_i$ . In simulations with a finite number of distinct processes it is more efficient to consider the groups of events according to their rates [28–30]. This can be done by forming lists of the same kinds of events according to the values of  $N_v$  in (3) of the first look-ahead rule or the values of  $N_c$  in (4) of the second look-ahead rule. This way we can put the total  $N$  events into  $(L + 1)$  lists, labelled by  $l = 0, \dots, L$ . All processes in the  $l$ -th list have the same rate  $r_l$ . We denote the number of processes in this list by  $n_l$ , which is called the *multiplicity*, and we have  $N = \sum_{l=0}^L n_l$ . To each list we assign a partial rate,  $R_l = n_l r_l$ , and a relative probability,  $P_l = R_l/R$ . Then the total rate is given by  $R = \sum_{l=0}^L n_l r_l$ . A fast list-based KMC algorithm at each step based on the grouping of events is given as follows.

*List-based KMC algorithm:*

Step 1: Generate a uniform random number,  $\xi_1 \in (0, 1)$  and decide which process will take place by choosing the list index  $s$  such that

$$\sum_{l=0}^{s-1} \frac{R_l}{R} < \xi_1 \leq \sum_{l=0}^s \frac{R_l}{R} \quad (5)$$

Step 2: Select a realization of the process  $s$ . This can be done with the help of a list of coordinates for each kind of event, and an integer random number  $\xi_2$  in the range  $[1, n_s]$ ;  $\xi_2$  is generated and the corresponding member from the list is selected.

Step 3: Perform the selected event leading to a new configuration.

Step 4: Use  $R$  and another random number  $\xi_3 \in (0, 1)$  to decide the time it takes for that event to occur (the transition time), i.e., the nonuniform time step  $\Delta t = -\log(\xi_3)/R$ .

Step 5: Update the multiplicity  $n_i$ , relative rates  $R_i$ , total rate  $R$  and any data structure that may have changed due to that event.

#### IV. NUMERICAL EXPERIMENTS

We next investigate 1D and 2D traffic flows in various parameter regimes with the numerical methods developed in the previous section. We start by calibrating some KMC model parameters with respect to well-known quantities from real traffic data.

##### A. Calibration and validity by the red light traffic problem

Following [21], we set the physical length of each cell to 22 feet, which allows for the average car length plus safe distance. Therefore, a mile (= 5280 feet) is equivalent to 240 cells. For a car which has an average speed of 60 miles per hour, an estimate of time to cross a cell is given by

$$\Delta t_{\text{cell}} = \frac{22 \text{ feet}}{60 \text{ miles/h}} = \frac{1 \text{ cell} \times 3600 \text{ secs}}{60 \times 240 \text{ cells}} = \frac{1}{4} \text{ sec.} \quad (6)$$

We calibrate the parameters  $\tau_0$  and  $E_c$  by simulating a free-flow regime and we expect all cars to drive at their desired speed that is set to 60 miles per hour. This is accomplished by setting the characteristic time  $\tau_0 = 0.25 \text{ sec}$ , and then  $\omega_0 = 4 \text{ sec}^{-1}$ . In fact, due to the stochasticity inherent in the simulations, sometimes cars may move faster or slower than the speed limit.

Fig. 2 shows the results of the “red light” traffic problem: the traffic light located at 0.5 miles (i.e.,  $x = 120$ ) is turned from red to green at the initial time and the “bumper to bumper” traffic wave is released. The initial condition is given by

$$\sigma_x(0) = \begin{cases} 1 & 1 \leq x \leq 120, \\ 0 & 120 < x \leq M. \end{cases} \quad (7)$$

The highway distance is set to 4 miles, i.e.,  $M = 960$  cells, which is large enough to ensure that finite-size effects do not interfere the simulations. Then the car density is  $120/960 = 12.5\%$ , which is in the free-flow regime. Given the initial conditions (7), we run  $K = 500$  simulations with different random number seeds and estimate the car density (middle panels in Fig. 2) by using ensemble averages with the formula

$$\rho(x, t) \approx \frac{1}{K} \sum_{k=1}^K \sigma_x^{(k)}(t) \quad (8)$$

where the integer  $k$  is the realization index. We also compute the variance in the car density over these simulations, shown in the bottom panels in Fig. 2.

We calibrate the potential strength  $E_c$  such that the velocity of a backward moving traffic jam can be approximately  $-10$  miles per hour, as estimated by traffic researchers in [31–33]. While we take the look-ahead parameter  $L = 4$  for both look-ahead rules, the calibrated value of the potential strength is  $E_c = 4.0$  for the first look-ahead rule (3) (left panels in Fig. 2) and  $E_c = 6.0$  for the second look-ahead rule (4) (right panels in Fig. 2).

##### B. Numerical comparisons of fluxes

To identify the range of significance of parameters, the interaction potential strength  $E_c$  and the look-ahead distance  $L$ , we make a series of numerical tests for different car densities with various values of parameters  $E_c$  and  $L$ . In the following we show the fundamental diagrams of the density-flow relationship and compare the results of different look-ahead rules (3) and (4). For these results we take a random car distribution at the initial time on a loop highway of 1 mile ( $M = 240$  cells) and observe the behavior of traffic flows as the car density increases incrementally. The traffic flow is measured as the number of cars passing a detector site per unit time [34]. Here we run each KMC simulation with different densities until the same final time (1 hour) and report long time averages of the flow in number of cars per hour.

Fig. 3 shows the results of the first look-ahead rule (3). We first examine how the potential strength  $E_c$  influences the traffic flow. In the left panel, we plot the microscopic flux for the look-ahead distance of  $L = 4$ , which is more appropriate for actual traffic conditions. As the potential strength increases, the concavity of traffic flow flux changes. In particular, when  $E_c \geq 3.0$  the flux is neither concave nor convex, which is similar to the simulation results and the observed data from [11, 17, 32]. This loss of convexity provides a richer behavior than the typical Lighthill-Whitham [35, 36] (or Burgers) type traffic model predicts. In the later case the flow-density curve is symmetric about the center  $\rho = 0.5$ , as shown by the trivial case of  $E_c = 0$ , where the maximum flux at  $\rho = 0.5$  is about 3600 cars per hour, as calculated via (9). Moreover, for given  $\rho$ , the magnitude of flux decreases with increasing  $E_c$  because the larger is the potential strength the stronger is the interaction to slowdown the cars.

In the right panel in Fig. 3, we show numerical results of the microscopic flux for different look-ahead distances  $L$  while keeping all other parameters fixed. The case of  $L = 4$  in the right panel connects to the case of  $E_c = 2.0$  in the left panel and allows for comparisons between the two. Note that, as  $L$  increases, the flux turns back to be concave. In particular, when  $L = 240$ , the flux of the KMC simulations agrees with that of the PDE in the typical Lighthill-Whitham type traffic model [35, 36]

$$F(\rho) = \omega_0 \rho(1 - \rho) \exp(-E_c). \quad (9)$$

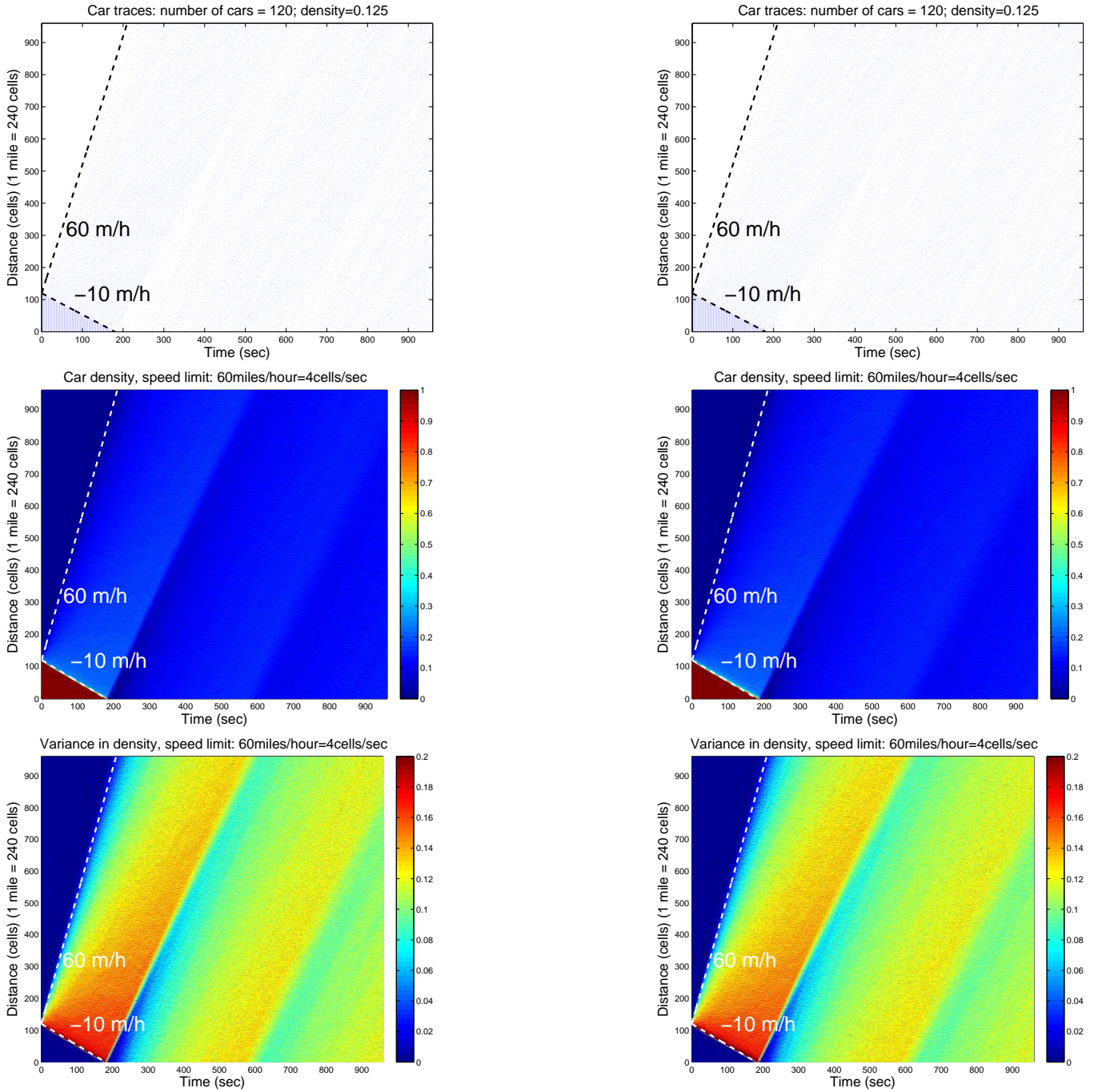


FIG. 2. Calibration of the potential strength  $E_c$  permitting a desired car speed of 60 miles per hour and a backward moving traffic jam velocity of  $\approx -10$  miles per hour. We take the highway distance of 4 miles ( $M = 960$  cells) and the look-ahead parameter of  $L = 4$  for both look-ahead rules. The initial condition corresponds to a red light traffic problem (i.e., bumper-to-bumper cars up to 0.5 miles (= 120 cells) and no cars after that, so total 120 cars in each simulation). The running time is up to 960 sec; (Left panels) Results of the first look-ahead rule (3) with the potential strength  $E_c = 4.0$ . (Right panels): Results of the second look-ahead rule (4) with the potential strength  $E_c = 6.0$ . (Top panels): Car traces in a single simulation; (Middle panels): Evolution of the car density averaged over 500 simulations; (Bottom panels): Evolution of the variance in the car density over 500 simulations.

The maximum flux at the center  $\rho = 0.5$  is about  $3600e^{-2.0} \approx 487$  cars per hour (recall that  $\omega_0 = 4\text{sec}^{-1}$ ).

Moreover, for given  $\rho$ , the magnitude of flux decreases with increasing  $L$  since the larger is the look-ahead dis-

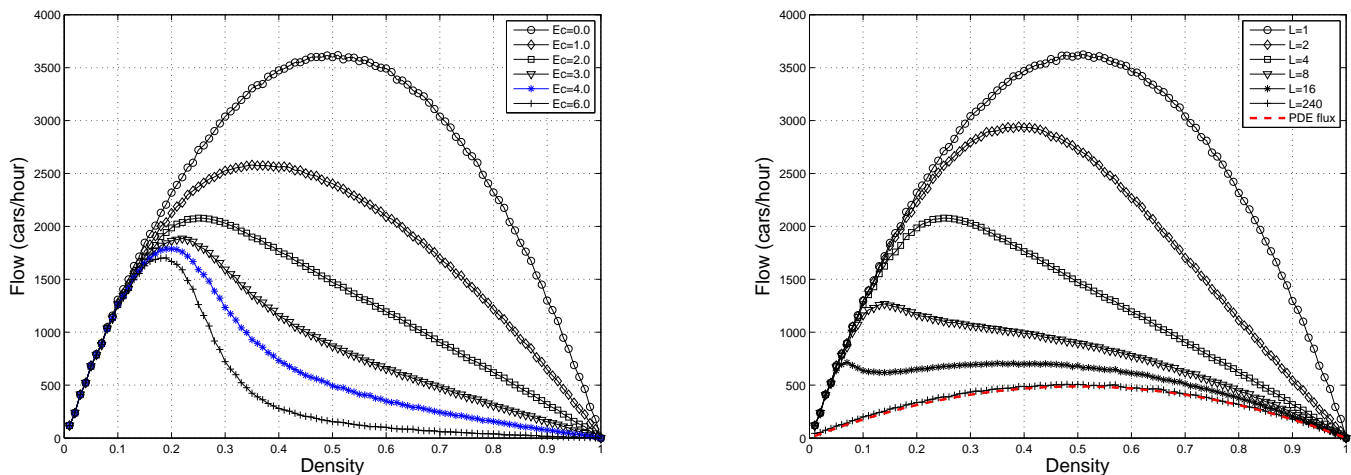


FIG. 3. Long time averages of the flow-density relationship for one-lane highway by using the first look-ahead rule (3). (Left panel): Comparison results of different values of the potential strength  $E_c$ . In these results we take the look-ahead parameter of  $L = 4$ . (Right panel): Comparison results of different values of the parameter  $L$ . In these results we use  $E_c = 2.0$ . Note that for long range interactions ( $L = 240$ ), the flux of the KMC simulation (shown in “+”) agrees with the PDE flux (9) (shown in the red dashed curve). In both results we take the highway distance of 1 mile ( $M = 240$  cells) and run all KMC simulations until the same final time (1 hour) before plotting the flux versus the car density.

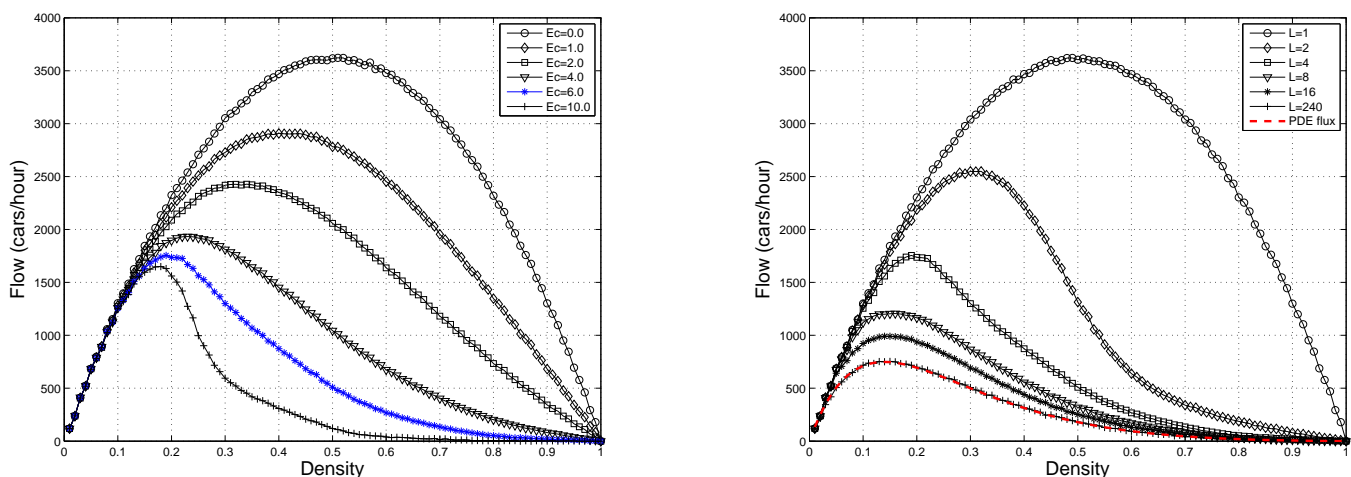


FIG. 4. Long time averages of the flow-density relationship for one-lane highway by using the second look-ahead rule (4). (Left panel): Comparison results of different values of the potential strength  $E_c$ . In these results we take the look-ahead parameter of  $L = 4$ . (Right panel): Comparison results of different values of the parameter  $L$ . In these results we use  $E_c = 6.0$ . Note that for long range interactions ( $L = 240$ ), the flux of the KMC simulation (shown in “+”) agrees with the PDE flux (10) (shown in the red dashed curve). As the same as in Fig. 3, in all KMC simulations the highway distance is 1 mile ( $M = 240$  cells) and the final time is 1 hour.

tance the longer is the effective range of interaction of the cars.

Fig. 4 shows the results of the second look-ahead rule (4). In the left panel, we again examine how the potential strength  $E_c$  influences the traffic flow with the look-ahead distance of  $L = 4$ . Here, we observe similar results as shown in the left panel in Fig. 3. For values of  $E_c \geq 4.0$  the flux is neither concave nor convex. Moreover, for given  $\rho$ , the magnitude of flux decreases with increasing

$E_c$ . The right panel in Fig. 4 displays numerical results of the microscopic flux for different look-ahead distances  $L$ , where the case of  $L = 4$  connects to the case of  $E_c = 6.0$  in the left panel. For the second look-ahead rule (4), as  $L$  increases, the flux turns to neither concave nor convex and the magnitude of flux also decreases. When  $L = 240$ , the flux of the KMC simulations matches with the following nonlocal flux of the PDE model [21]

$$F(\rho) = \omega_0 \rho(1 - \rho) \exp(-E_c \bar{\rho}). \quad (10)$$

where  $\bar{\rho}$  is the average of  $\rho$  on the long range  $L$  (if  $L = 240$ ,  $\bar{\rho} = \rho$ ). Since physically we do not expect that drivers would (or even could) have a perception of traffic up front for many cars, both look-ahead rules (3) and (4) are reasonable for small  $L$ .

We note that in the left panels in Figs. 3 and 4, the density-flow curve of the KMC simulation (shown in blue “\*”) clearly displays that the region of free-flow is up to the density of approximately  $\rho_{\text{crit}} = 0.2$ , i.e.,  $240 \times 0.2 \approx 50$  cars per mile. This result is naturally produced by the traffic dynamics in our simulations with the calibrated parameters  $\tau_0 = 0.25\text{sec}$ , and  $E_c = 4.0$  or  $6.0$  for each look-ahead rule, respectively. We also observe a maximum traffic flow of approximately 1800 cars per hour as we take the car desired speed of 60 miles per hour, which should agree with observations of the flow of 2000 cars per hour with the desired speed of 65 miles per hour [32, 37].

### C. Numerical results of time-headway distributions

The time-headway (TH) is defined as the time interval between the departures (or arrivals) of two successive cars recorded by a fixed detector on the highway [34]. The TH distribution is regarded as an important characteristic of traffic flow since the TH distribution contains more detailed information on traffic flow than that available from the flux alone. Actually the flux  $J$  can be estimated by  $J = 1/T_{\text{ave}}$  where  $T_{\text{ave}}$  is the average of TH [34]. With the variation of density  $\rho$  of the cars,  $T_{\text{ave}}$  comes to a minimum at  $\rho = \rho_{\text{crit}}$ , where the flux reaches its maximum. As shown in the bottom panels in Fig. 5,  $T_{\text{ave}}$  takes the minimum, 2.0sec, at  $\rho_{\text{crit}} = 0.2$  in both cases, which gives the maximum traffic flow of  $J = 3600/2.0 = 1800$  cars per hour.

Fig. 5 shows the results of the first and second look-ahead rules (3) and (4) with the potential strength  $E_c = 4.0$  and  $E_c = 6.0$ , respectively. In both results we take the look-ahead distance  $L = 4$  and obtain similar distributions. As shown in top panels in Fig. 5, the TH distributions of cases  $\rho = 0.1, 0.2$  and  $0.3$  show a strong peak around  $2.0 \sim 3.0\text{sec}$ , which represents the global maximum of the distribution. These short THs correspond to some groups of cars moving very fast and their drivers are facing the risk of driving “bumper to bumper” with a rather high speed. However, the corresponding high-flow states exhibit metastability, in which a perturbation of finite magnitude and duration can break down the high-flow [31]. As the density  $\rho$  increases in the regime of congested traffic ( $\rho > 0.3$ ), the small THs have less weight in the TH distributions. In “stop-and-go” traffic ( $\rho \geq 0.7$ ), short THs are suppressed (results not shown). The bottom panels in Fig. 5 also show that the average of TH,  $T_{\text{ave}}$  becomes longer as the density  $\rho$  increases.

### D. Traffic flows on 2D lattice

In this subsection we extend the traffic model from 1D to 2D lattices and study traffic in cities. Our 2D model is closely related to the Biham-Middleton-Levine (BML) model [38], which is the earliest CA model of traffic in idealized networks of streets in cities. Although the model is simple, it displays very complex phenomena, e.g., phase transition and self-organization. Since then, extensive researches have been done based on this model and it serves as a theoretical benchmark for modelling urban traffic [39–51].

In the original BML model, two species of cars, eastbound and northbound, populate a 2D periodic square lattice. Each lattice site can be in one of three states: empty, occupied by an eastbound car ( $\rightarrow$ ), or occupied by a northbound car ( $\uparrow$ ). All the streets parallel to the  $x$ -direction of a Cartesian coordinate system are assumed to allow only single-lane eastbound traffic while all those parallel to the  $y$ -direction allow only single-lane northbound traffic. The states of eastbound cars are updated in parallel at every odd time step whereas those of the northbound cars are updated in parallel at every even time step following a rule: a car advances one lattice site if and only if the target site is currently empty, otherwise the car remains stationary even if the target site is to become empty during the same time step. The dynamics is fully deterministic and the randomness in this model enters only through the initial random distribution of cars. Furthermore, the number of cars on every street is conserved since no turning of the vehicles is allowed by the updating rules. Therefore, on an  $M \times M$  lattice, there are  $2M$  conservation laws on 1D strips. Suppose,  $N_{\rightarrow}$  and  $N_{\uparrow}$  are the numbers of the eastbound and northbound cars, respectively, in the initial state of the system. The densities of the eastbound and northbound cars are given by  $\rho_{\rightarrow} = N_{\rightarrow}/M^2$  and  $\rho_{\uparrow} = N_{\uparrow}/M^2$ , respectively, while the global density of the cars is  $\rho = \rho_{\rightarrow} + \rho_{\uparrow}$ . In this study we will focus on the symmetric cases with equal densities, i.e.,  $\rho_{\rightarrow} = \rho_{\uparrow} = \rho/2$ .

Here, instead of using the parallel updating rule in the original BML model, we take the look-ahead rules to describe the car movements on each street in the same manner as in the 1D lattice model in Section 2. Then, we follow the prescriptions of the 1D model for describing the positions and speeds of the cars as well as for taking into account the interactions between the cars on the same street with the characteristic time  $\tau_0$ , the interaction potential strength  $E_c$ , and the look-ahead parameter  $L$ .

To study the 2D models with the two look-ahead rules, we have performed a series of simulations for different car densities with various values of the look-ahead parameter  $L$  and the lattice size  $M$ . We fix the potential strength  $E_c = 4.0$  and  $E_c = 6.0$  for the first and second look-ahead rules (3) and (4), respectively. The results exhibit a phase transition from the free-flow regime to the completely jammed regime as the car density increases.

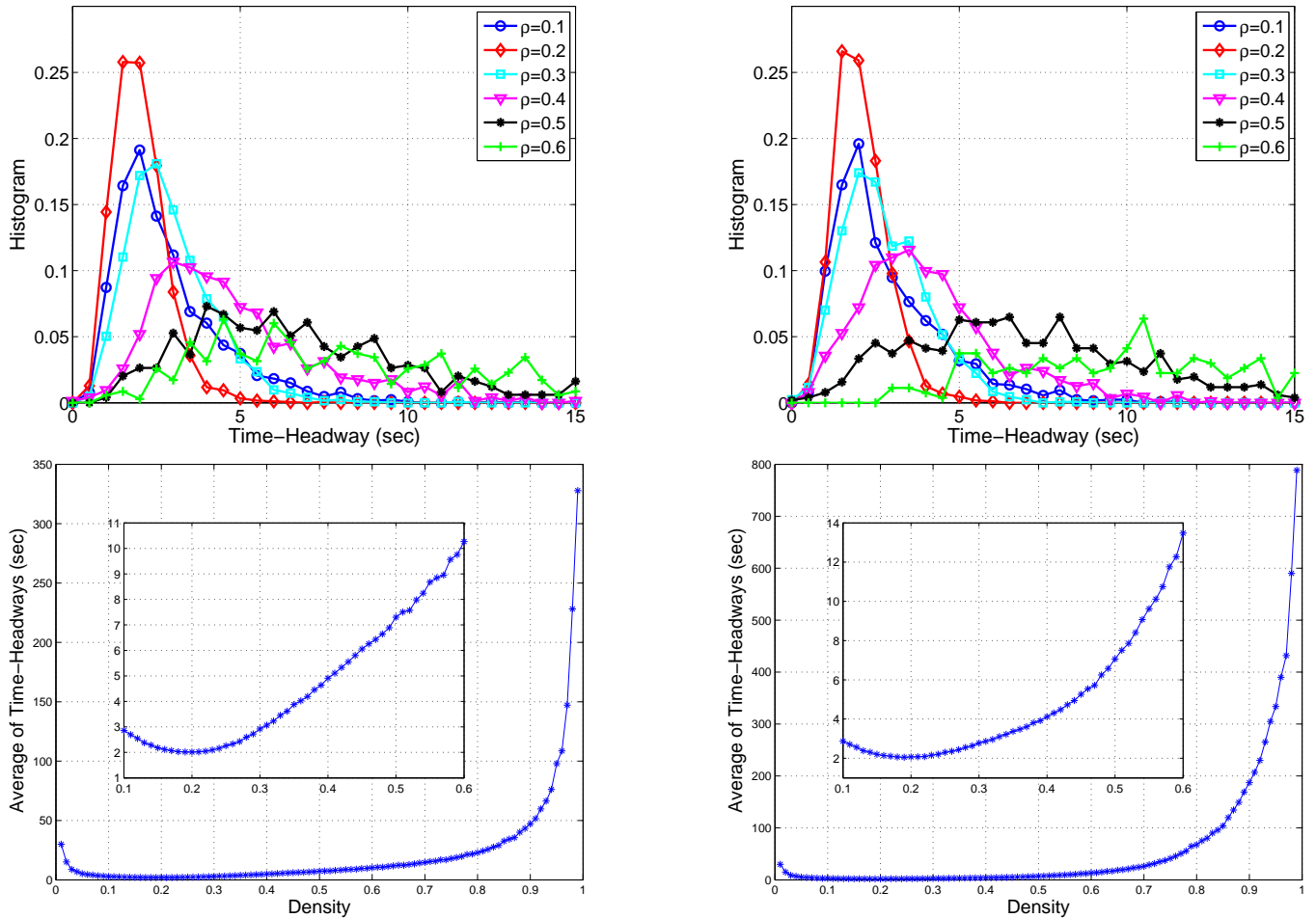


FIG. 5. (Top panels): Time-headway (TH) distributions for different car densities from  $\rho = 0.1$  to  $0.6$ . (Bottom panels): Average of TH,  $T_{\text{ave}}$ , versus the car density  $\rho$ . (Left panels): Results of the first look-ahead rule (3) with the parameter  $L = 4$  and the potential strength  $E_c = 4.0$ . (Right panels): Results of the second look-ahead rule (4) with with the parameter  $L = 4$  and the potential strength  $E_c = 6.0$ . As the same as in Fig. 3, in all KMC simulations the highway distance is 1 mile ( $M = 240$  cells) and the final time is 1 hour. The insets in the bottom panels show that  $T_{\text{ave}}$  takes the minimum, 2.0sec, at  $\rho_{\text{crit}} = 0.2$  in both cases.

Fig. 6 shows three typical configurations of the 2D model on an  $M \times M$  lattice of size  $M = 256$  using the first look-ahead rule (3) with the parameter  $L = 4$  and the potential strength  $E_c = 4.0$ . The left panel displays a configuration below the transition, i.e., the free-flow phase with a low car density  $\rho = 0.06$ , where the cars are distributed randomly and homogenously. The middle panel shows a completely jammed phase with  $\rho = 0.11$  above the transition. Here all the cars are stopped in a global jam, which is oriented along the diagonal from the lower-left to the upper-right corners. This way it blocks the paths of all cars which finally get stopped. The intrinsic stochasticity of the dynamics triggers the onset of jamming and the phenomenon of complete jamming through self-organization as well as the final jammed configurations are similar to those in the BML model. The right panel shows a high density, randomly jammed phase

with  $\rho = 0.6$ , in which small jams appear simultaneously all over the lattice and connect almost immediately with other jams, stopping all cars. In this phase, the system has no time to self-organize, and instead of one global jam, we observe a collection of small random jams. We note that the configurations using the second look-ahead rule (4) with  $L = 4$  and  $E_c = 6.0$  are not shown since they are similar to those in Fig. 6.

For critical phenomena, it is expected that the size of the system plays an important role. Therefore, we analyze the effects of the lattice size  $M$  on the 2D traffic with the diagrams of density-flow and density-velocity relationships. Here we run all KMC simulations with different densities ranging from  $\rho = 0$  to  $\rho = 0.16$  until the same final time (5 hours). For each simulation we compute long time averages of the flow in number of cars per hour per lane and obtain the ensemble-average

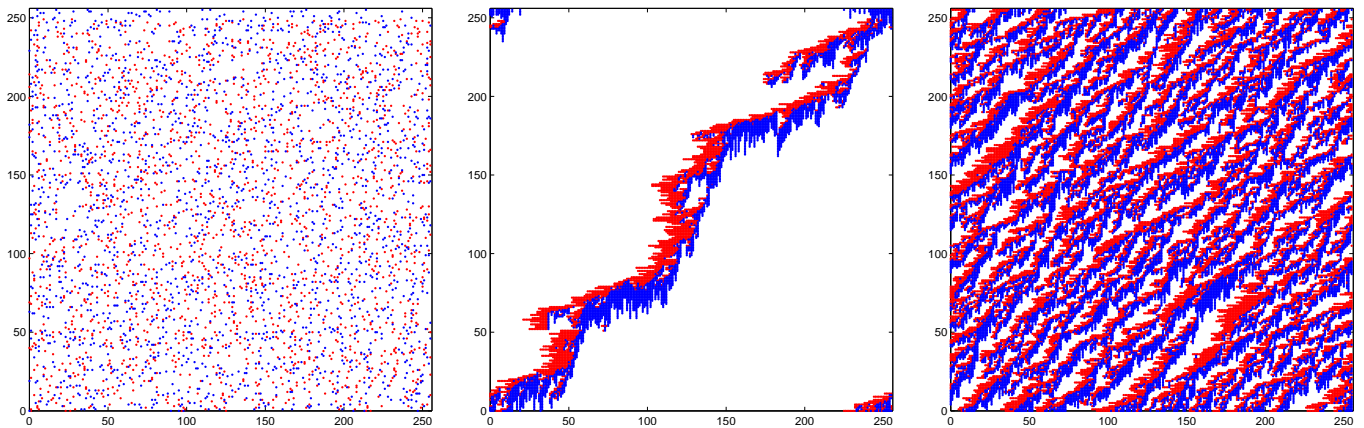


FIG. 6. Typical configurations of the 2D traffic model on an  $M \times M$  lattice of size  $M = 256$  using the first look-ahead rule (3) with the parameter  $L = 4$  and the potential strength  $E_c = 4.0$ . The eastbound and northbound cars are represented by red and blue dots, respectively. (Left panel): The free-flow phase with a low car density  $\rho = 0.06$ . (Middle panel): The completely jammed phase consisting of one global jam with the car density  $\rho = 0.11$ . (Right panel): A high density, randomly jammed phase with  $\rho = 0.6$ .

velocity in cells per second by averaging the velocities over all cars moving in the same direction, eastbound or northbound. Due to the symmetry with equal densities of two species, i.e.,  $\rho_{\rightarrow} = \rho_{\uparrow} = \rho/2$ , the results of both directions are almost same, so we only report the results of eastbound cars. Moreover, for every value of  $\rho$  and  $M$ , ten simulations with different random number seeds are averaged over.

Results of four system sizes from  $64 \times 64$  to  $512 \times 512$  are presented in each panel in Fig. 7. Every curve exhibits a reasonably sharp phase transition between the free-flow phase and the jammed phase. As shown in both top panels, in the free-flow regime the flux increases as the car density  $\rho$  increases, and reaches its maximum at the critical value,  $\rho_{\text{crit}}$ . Beyond that point, the phase transition starts and the flux drops down quickly to zero as all cars are stopped. On the other hand, the bottom panels show that in the free-flow regime the ensemble-average velocity decreases slowly from the maximum speed limit of 4 cells per second (i.e., 60 miles per hour) as  $\rho$  increases and the chance of interaction between cars gets higher. When  $\rho$  is larger than the critical point  $\rho_{\text{crit}}$ , the average velocity also drops down quickly to zero. We observe that as the system size increases, the transition becomes sharper and the value of  $\rho_{\text{crit}}$  tends to decrease. However, as in the BML model, currently we are not able to determine whether  $\rho_{\text{crit}}$  converges to a finite value or to zero in the infinite system limit. We also note that the results of the first look-ahead rule (3) with  $E_c = 4.0$  (in left panels) and those of the second rule (4) with  $E_c = 6.0$  (in right panels) are similar, which indicates that both rules are reasonable for small  $L = 4$ .

However, Fig. 8 shows that when  $L \geq 8$ , two look-ahead rules produce different results of both diagrams of density-flow and density-velocity relationships. As shown in the top-left panel for the first rule (3) with  $E_c = 4.0$

and different values of the look-ahead parameter  $L = 1$  to 256, the value of the critical car density  $\rho_{\text{crit}}$  of the transition decreases as the parameter  $L (\geq 2)$  increases. Moreover, the magnitude of maximum flux decreases dramatically with increasing  $L$ . In particular, for the cases of  $L = 128$  and 256, the flux is almost suppressed. In all cases of  $L \leq 16$ , the flux increases as  $\rho$  increases, and reaches the maximum at  $\rho_{\text{crit}}$ , then the flux drops down quickly to zero. On the other hand, in the cases of  $L \geq 32$ , the flux decreases slowly after it reaches its maximum. The bottom-left panel shows that in each case of  $L \leq 16$ , the ensemble-average velocity decreases slowly with the increase of  $\rho$  before the transition. After that, the average velocity drops down quickly to zero. But in the cases of  $L \geq 64$ , the average velocity decreases quickly from the beginning.

The right panels in Fig. 8 show the results of the second look-ahead rule (4) with the potential strength  $E_c = 6.0$  and different values of the look-ahead parameter  $L = 1$  to 256. As shown in the top-right panel, the value of the critical car density  $\rho_{\text{crit}}$  of the transition increases as the parameter  $L (\leq 64)$  increases. On the other hand, for the cases of  $L > 64$ , the value of  $\rho_{\text{crit}}$  of the transition decreases as the parameter  $L$  increases. For all cases with different values of  $L$ , the flux increases as  $\rho$  increases until  $\rho_{\text{crit}}$  when the transition happens, and then the flux drops down quickly to zero. The magnitude of maximum flux decreases slowly with increasing  $L$ . The bottom-right panel shows that in all cases of  $L$ , the ensemble-average velocity decreases slowly with the increase of  $\rho$  until the transition appears and then drops down quickly to zero.

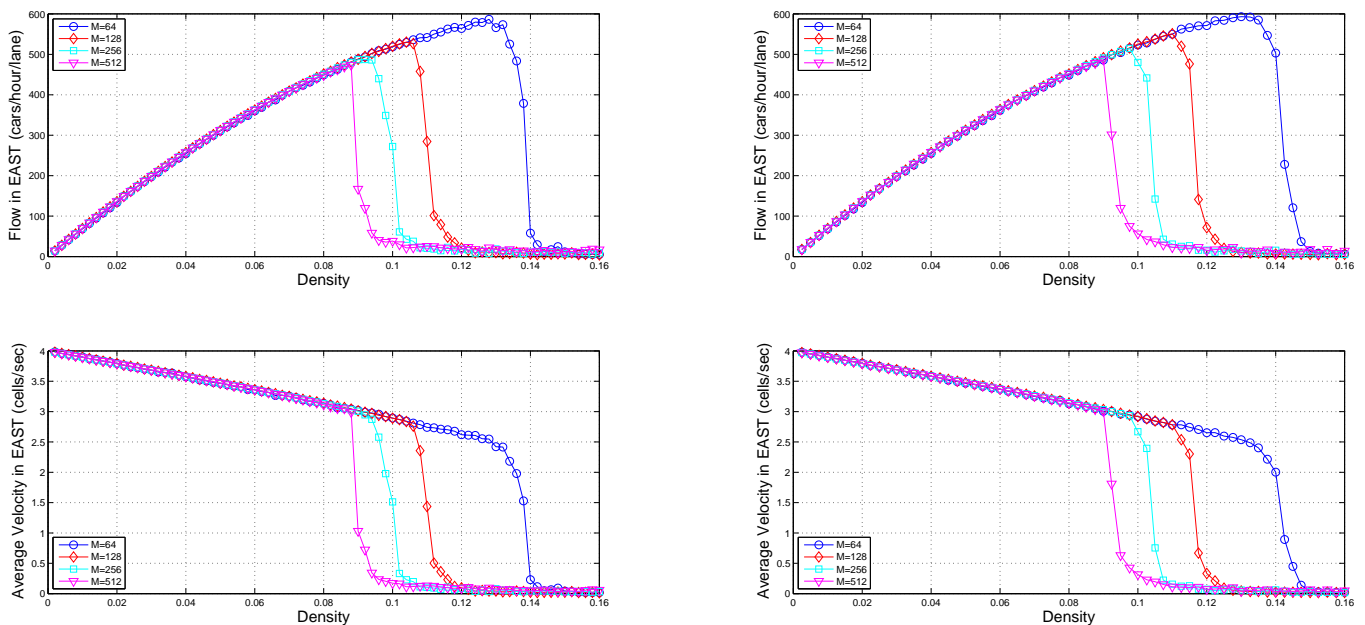


FIG. 7. Comparison results of the 2D traffic model with four different system sizes from  $64 \times 64$  to  $512 \times 512$ . (Top panels): Long time averages of the flow-density relationship of eastbound cars. (Bottom panels): Ensemble-average velocity of eastbound cars versus the car density  $\rho$ . (Left panels): Results of the first look-ahead rule (3) with the potential strength  $E_c = 4.0$  and  $L = 4$ . (Right panels): Results of the second look-ahead rule (4) with the potential strength  $E_c = 6.0$  and  $L = 4$ . In all KMC simulations the final time is 5 hours.

## V. CONCLUSIONS

We have used the kinetic Monte Carlo (KMC) method with a lattice model to study 1D and 2D traffic flows. Our work is motivated by the growing need to understand the mechanisms leading to traffic jams and design and optimize transportation systems. This cellular automata (CA) traffic model defines stochastic rules for the movement of cars by using the look-ahead potential of each car. In particular, we used two different look-ahead rules: one is based on the distance from the car under consideration to the car in front of it; the other one is based on the density of cars ahead.

To simulate the time evolution of the traffic system, we developed an efficient list-based KMC algorithm using fast search that can further improve computational efficiency. In the KMC method, the dynamics of cars in the traffic system is described in terms of the transition rates corresponding to possible configurational changes of the system, and then the corresponding time evolution of the system can be expressed in terms of these rates. The KMC simulations relied on the calibration of three model parameters: the characteristic time  $\tau_0$ , the interaction potential strength  $E_c$ , and the look-ahead parameter  $L$ . After calibration against empirical results from real traffic, the KMC simulations are used to quantitatively predict the time evolution of 1D and 2D traffic flows. The results of our model are comparable to those from other well-known traffic flow models and the cor-

responding empirical results from real traffic in certain parameter regimes.

For 1D traffic flows (in one-lane), we obtained fundamental diagrams with qualitatively meaningful flows which display many of the observed traffic states. Comparison of the 1D numerical results of the two look-ahead rules shows that in long-range interactions limit with large look-ahead parameter  $L$ , the two rules produce different coarse-grained macroscopic limits in the form of integro-differential Burgers equations. But for small  $L$ , both rules produce similar results. The 2D results of both rules exhibit a sharp phase transition from freely flowing to fully jammed, as a function of initial density of cars. Again, both rules produce different 2D results in long-range interactions limit with large  $L$ , but the results of small  $L$  are similar. Moreover, currently we do not expect that drivers would really (or even could) have a perception of traffic up front for many cars, thus both rules are reasonable for small  $L$ .

It is possible to improve our 1D and 2D model further in the following directions. We can include entrances and exits in 1D model by adding dynamics mechanisms such as adsorption/desorption. In reality, at places with traffic jams, drivers may take a turn around the street and bypass the busy spot. Thus, in more realistic 2D models, we can introduce the possibility of turning an eastbound car into a northbound car, vice versa. We also need to consider nonsymmetric cases with unequal densities of eastbound and northbound cars. More com-

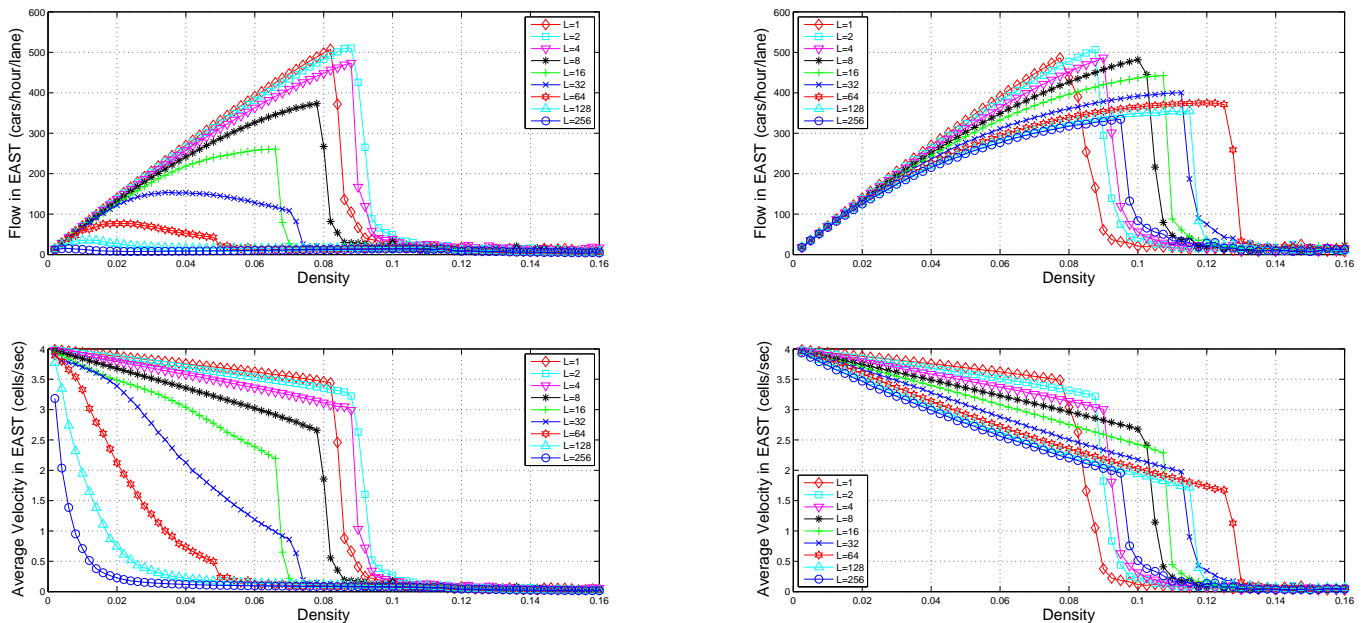


FIG. 8. Comparison results of different values of the look-ahead parameter from  $L = 1$  to  $L = 256$  for the 2D traffic model with the system size  $512 \times 512$ . (Top panels): Long time averages of the flow-density relationship of eastbound cars. (Bottom panels): Ensemble-average velocity of eastbound cars versus the car density  $\rho$ . (Left panels): Results of the first look-ahead rule (3) with the potential strength  $E_c = 4.0$ . (Right panels): Results of the second look-ahead rule (4) with the potential strength  $E_c = 6.0$ . In all KMC simulations the final time is 5 hours.

plicated models addressing these aspects will be explored in the future.

## ACKNOWLEDGMENTS

The author would like to thank Drs. Russ Caflisch, Tong Li and Alexandros Sopasakis for useful discussions. Y. Sun would like to thank the NSF funded Mathematical Biosciences Institute (MBI) at the Ohio State University, where part of this work was carried out. Sun is partially supported by a USC startup fund, a SC EP-SCoR GEAR Award, and an Early Career Award from MBI. Timofeyev is partially supported by the NSF Grant DMS-1109582.

- 
- [1] K. NAGEL, J. ESSER, M. RICKERT, in: D. Stauffer (Ed.), *Ann. Rev. Comp. Phys.*, World Scientific, Singapore, 1999.
- [2] D. CHOWDHURY, L. SANTEN, AND A. SCHADSCHNEIDER, *Statistical physics of vehicular traffic and some related systems*, *Physics Reports*, **329** (2000), pp. 199–329.
- [3] D. HELBING, *Traffic and related self-driven many-particle systems*, *Rev. Mod. Phys.*, **73** (2001), pp. 1067–1141.
- [4] T. NAGATANI, *The physics of traffic jams*, *Rep. Prog. Phys.*, **65** (2002), pp. 1331–1386.
- [5] N. BELLOMO AND C. DOGBE, *On the modeling of traffic and crowds: A survey of models, speculations, and perspectives*, *SIAM Review*, **53** (2011), pp. 409–463.
- [6] A. SCHADSCHNEIDER, D. CHOWDHURY, AND K. NISHINARI, *Stochastic Transport in Complex Systems*, Elsevier, The Netherlands, 2011.
- [7] L. A. PIPES, *An Operational Analysis of Traffic Dynamics*, *J. Appl. Phys.*, **24** (1953), pp. 274–281.
- [8] G. F. NEWELL, *Nonlinear effects in the dynamics of car following*, *Oper. Res.* **9** (1961), pp. 209–229.
- [9] M. BANDO, K. HASEBE, A. HAKAYAMA, A. SHIBATA, AND Y. SUGIYAMA, *Dynamical model of traffic congestion and numerical simulation*, *Phys. Rev. E*, **51** (1995), pp. 1035–1042.
- [10] M. CREMER AND J. LUDWIG, *A fast simulation model for traffic flow on the basis of Boolean operation*, *Math. Comput. Simulation*, **28** (1986), pp. 297–303.
- [11] K. NAGEL AND M. SCHRECKENBERG, *A cellular automaton model for freeway traffic*, *J. Phys. I France*, **2** (1992), pp. 2221–2229.

- [12] S. WOLFRAM, *Cellular Automata and Complexity*, Addison-Wesley, Reading, MA, 1994.
- [13] K. NAGEL AND M. PACZUSKI, *Emergent traffic jams*, Phys. Rev. E, **51** (1995), pp. 2909–2918.
- [14] R. BARLOVIC, L. SANTEN, A. SCHADSCHNEIDER, AND M. SCHRECKENBERG, *Metastable states in cellular automata for traffic flow*, Eur. J. Phys. B, **5** (1998), pp. 793–800.
- [15] W. KNOSPE, L. SANTEN, A. SCHADSCHNEIDER, AND M. SCHRECKENBERG, *Towards a realistic microscopic description of highway traffic*, J. Phys. A, **33** (2000), pp. L477–L485.
- [16] W. KNOSPE, L. SANTEN, A. SCHADSCHNEIDER, AND M. SCHRECKENBERG, *Single-vehicle data of highway traffic: Microscopic description of traffic phases*, Phys. Rev. E, **65** (2002), paper 056133.
- [17] T. LI, *Nonlinear dynamics of traffic jams*, Physica D, **207** (2005), pp. 41–51.
- [18] P. NELSON, *On two-regime flow, fundamental diagrams and kinematic-wave theory*, Transportation Sci., **40** (2006), pp. 165–178.
- [19] M. KATSOULAKIS, A. MAJDA, AND A. SOPASAKIS, *Multiscale couplings in prototype hybrid deterministic/stochastic systems: Part I, deterministic closures*, Comm. Math. Sci., **2** (2004), pp. 255–294.
- [20] M. KATSOULAKIS, A. MAJDA, AND A. SOPASAKIS, *Multiscale couplings in prototype hybrid deterministic/stochastic systems: Part II, stochastic closures*, Comm. Math. Sci., **3** (2005), pp. 453–478.
- [21] A. SOPASAKIS AND M. A. KATSOULAKIS, *Stochastic modeling and simulation of traffic flow: Asymmetric single exclusion process with Arrhenius look-ahead dynamics*, SIAM J. Appl. Math., **66** (2006), pp. 921–944.
- [22] N. DUNDON AND A. SOPASAKIS, *Stochastic modeling and simulation of multi-lane traffic*, Transp. Traffic Theory, **17** (2007), pp. 661–689.
- [23] T. ALPEROVICH AND A. SOPASAKIS, *Stochastic description of traffic flow*, J. Stat. Phys., **133** (2008), pp. 1083–1105.
- [24] C. HAUCK, Y. SUN, I. TIMOFEYEV *On cellular automata models of traffic flow with look ahead potential*, Stochastics and Dynamics, in review.
- [25] A. B. BORTZ, M. H. KALOS, AND J. L. LEBOWITZ, *A new algorithm for Monte Carlo simulation of Ising spin systems*, J. Comput. Phys., **17** (1975), pp. 10–18.
- [26] N. METROPOLIS, A. E. ROSENBLUTH, M. N. ROSENBLUTH, A. H. TELLER AND E. TELLER *Equation of state calculations by fast computing machines*, J. Chem. Phys., **21** (1953), pp. 1087–97.
- [27] T. D. LIGGETT, *Interacting Particle Systems*, Springer, Berlin, 1985.
- [28] J. L. BLUE, I. BEICHL, AND F. SULLIVAN, *Faster Monte Carlo simulations*, Phys. Rev. E, **51** (1995), paper R867.
- [29] T. P. SCHULZE, *Kinetic Monte Carlo simulations with minimal searching*, Phys. Rev. E, **65** (2002) paper 036704.
- [30] Y. SUN, R. CAFLISCH, AND B. ENGQUIST, *A multiscale method for epitaxial growth*, SIAM Multiscale Model. Simul., **9** (2011), pp. 335–354.
- [31] B. S. KERNER AND H. REHBORN, *Experimental properties of phase transitions in traffic flow*, Phys. Rev. Lett., **79** (1997), pp. 4030–4033.
- [32] D. HELBING, A. HENNECKE, V. SHVETSOV, AND M. TREIBER, *Micro- and macro-simulation of freeway traffic*, Math. Comput. Modelling, **35** (2002), pp. 517–547.
- [33] A. SCHADSCHNEIDER, *Traffic flow: A statistical physics point of view*, Phys. A, **312** (2002), pp. 153–187.
- [34] A. D. MAY, *Traffic Flow Fundamentals*, Prentice-Hall, Englewood Cliffs, NJ, 1990.
- [35] M. LIGHTHILL AND G. WHITHAM, *On kinematic waves. II. A theory of traffic flow on long crowded roads*, Proc. Roy. Soc. London. Ser. A., **229** (1955), pp. 317–345.
- [36] G. B. WHITHAM, *Linear and Nonlinear Waves*, Wiley-Interscience, New York, 1974.
- [37] K. NAGEL, D. E. WOLF, P. WAGNER, AND P. SIMON, *Two-lane traffic rules for cellular automata: A systematic approach*, Phys. Rev. E, **58** (1998), pp. 1425–1437.
- [38] O. BIHAM, A. MIDDLETON, AND D. LEVINE, *Self-organization and a dynamical transition in traffic-flow models*, Phys. Rev. A, **46** (1992), paper R6124.
- [39] T. NAGATANI, *Jamming transition in the traffic-flow model with two-level crossings*, Phys. Rev. E, **48** (1993), pp. 3290–3294.
- [40] T. NAGATANI, *Anisotropic effect on jamming transition in traffic-flow model*, J. Phys. Soc. Jpn., **62** (1993), pp. 2656–2662.
- [41] J. A. CUESTA, F. C. MARTINEZ, J. M. MOLERA, AND A. SANCHEZ, *Phase transitions in two-dimensional traffic-flow models*, Phys. Rev. E, **48** (1993), pp. R4175–R4178.
- [42] K. H. CHUNG, P. M. HUI AND G. Q. GU, *Two-dimensional traffic flow problems with faulty traffic lights*, Phys. Rev. E, **51** (1995), pp. 772–774.
- [43] J. M. MOLERA, F. C. MARTINEZ, J. A. CUESTA, AND R. BRITO, *Theoretical approach to two-dimensional traffic flow models*, Phys. Rev. E, **51** (1995), pp. 175187.
- [44] D. CHOWDHURY AND A. SCHADSCHNEIDER, *Self-organization of traffic jams in cities: Effects of stochastic dynamics and signal periods*, Phys. Rev. E, **59** (1999), pp. R1311–R1314.
- [45] E. BROCKFELD, R. BARLOVIC, A. SCHADSCHNEIDER AND M. SCHRECKENBERG, *Dynamical model of traffic congestion and numerical simulation*, Phys. Rev. E, **64** (2001), paper 056132.
- [46] R. M. D’SOUZA *Coexisting phases and lattice dependence of a cellular automaton model for traffic flow*, Phys. Rev. E, **71** (2005), paper 066112.
- [47] R. M. D’SOUZA *BML revisited: Statistical physics, computer simulation, and probability*, Complexity, **12** (2006), pp. 30–39.
- [48] N. J. LINESCH AND R. M. D’SOUZA, *Periodic states, local effects and coexistence in the BML traffic jam model*, Physica A, **387** (2008), pp. 6170–6176.
- [49] Z. J. DING, R. JIANG AND B. H. WANG, *Phase transitions in two-dimensional traffic-flow models*, Phys. Rev. E, **83** (2011), paper 047101.
- [50] Z. J. DING, R. JIANG, W. HUANG AND B. H. WANG, *Phase transitions in two-dimensional traffic-flow models*, J. Stat. Mech., (2011), paper 06017.
- [51] Z. J. DING, R. JIANG, M. LI, Q. LI AND B. H. WANG, *Effect of violating the traffic light rule in the Biham-Middleton-Levine traffic flow model*, Europhys. Lett., (2012), paper 68002.